Journal of Orthopaedic Surgery and Research

RESEARCH

Open Access

Biomechanical changes in lumbar intervertebral discs after percutaneous endoscopic transforaminal discectomy surgery at different Body Mass Index (BMI) categories

Xiaohai Zhang[1,2], Jinghui Lin[3], Chen Liu[4], Shuangtao Xue[2], Mengying Wu[2] and Zongsheng Yin[1*]

Abstract

Objective Percutaneous Endoscopic Transforaminal Discectomy (PETD) is recognized as the leading surgical intervention for lumbar disc herniation (LDH). Moreover, Body Mass Index (BMI) has been established as an independent risk factor for disc reherniation post-PETD. Furthermore, there is a lack of studies investigating the biomechanical changes in the disc post-PETD in relation to diverse BMI levels.

Methods A three-dimensional nonlinear finite element model was developed to simulate the L3-S1 lumbar spine, and a surgical model of the lumbar 4/5 right PETD was also constructed. Forces of 392 N (BMI 20.76 kg/m^2), 457 N (24.22 kg/m^2), 523 N (27.68 kg/m^2), 588 N (31.14 kg/m^2) and 653 N (34.6 kg/m^2) were applied from the superior edge of the L3 vertebrae. The equivalent von Mises stresses and maximum deformation of the L4/5 nucleus pulposus were observed in normal group and PETD surgery group.

Results We established normal and PETD surgery model with different BMIs, contributes to understand the equivalent von Mises stresses and maximum deformation of the L4/5 nucleus pulposus with different BMI. The results indicated that the rise in BMI correlates with heightened equivalent von Mises stresses and maximum deformation within the L4/5 nucleus pulposus in both in normal group and PETD surgery group. Besides, the von Mises stress and maximum deformation of the NP in flexion loading are significantly higher than in other loading conditions under the same BMI condition. These values, alongside the occurrence of high-stress areas, display fluctuations across distinct postures, under the influence of BMI. Furthermore, a discernible accumulation of stress was noted within the compromised regions of the nucleus pulposus.

Conclusion The study suggested that patients who undergone PETD surgery should refrain from engaging in strenuous activities especially flexion during early rehabilitation through finite element analysis. For patients with a

*Correspondence:
Zongsheng Yin
yinzongsheng@sina.com

Full list of author information is available at the end of the article

high BMI, it is advisable to scientifically reduce weight before and after the surgery in order to maintain appropriate stress on the intervertebral disc.

Keywords Finite element analysis, Percutaneous endoscopic transforaminal discectomy, Disc recurrence, Biomechanical changes, Body Mass Index

Introduction

Lumbar Disc Herniation (LDH) represents a pathological condition characterized by lumbar disc damage or prolapse, leading to the extrusion of its gel-like material and subsequent compression of nearby nerve roots, spinal nerves, or the spinal cord. This compression manifests as a spectrum of clinical symptoms, encompassing low back pain, hip discomfort, and radiating pain in the lower extremities. The prevalence of herniated discs varies from 1.4 to 20% [1,2]. A wide range of treatment modalities are available for herniated discs, encompassing conservative approaches such as pharmacotherapy, transforaminal epidural steroid injections, exercise regimens, manipulative therapies, and traction therapy. In the event that conservative measures prove ineffective, surgical interventions may be considered, including vertebral plate decompression, microscopic discectomy, percutaneous endoscopic transforaminal discectomy (PETD), and lumbar spine fusion via posterior decompression [3,4]. Empirical research and evidence-based medicine underscore the superior outcomes associated with PETD, evidenced by reduced reliance on pain medications, mitigated trauma, and alleviated financial strain on patients [5].

In comparison to traditional open surgery and endoscopic nucleotomy, patients undergoing PETD surgery exhibit higher rates of postoperative recurrence, occurring earlier, significantly impacting clinical prognosis [6]. *Suk et al.* [7] defined recurrent lumbar disc herniation (RLDH) as the reappearance of disc protrusion at the operated segment after a pain-free or relieved period of at least 6 months postoperatively, which has since been widely adopted by most scholars as the diagnostic criterion for RLDH. *Lee et al.* [8] indicated that approximately 60–80% of patients diagnosed as RLDH experience recurrence within 6 months after first PTED surgery. Previous literature had reported various factors influencing RLDH, including age, BMI, occupation, smoking status, location, type, degeneration degree of disc herniation, lumbar segment mobility, and surgeon's learning curve, yet their conclusions remain contentious [9,10]. Among the myriad factors contributing to recurrence, BMI serves was regarded as an independent recurrence factor of intervertebral disc degeneration [11]. Study with medium-quality (class II or III) evidence showed that postoperative LDH recurrence was significantly correlated with obesity (BMI≥25 kg/m^2). In a separate study investigating the factors contributing to disc recurrence, it was determined that the mean BMI value in the recurrence group was 24.9 kg/m^2, while the mean BMI value in the non-recurrence group was 22.9 kg/m^2 [12–14]. The influence of diverse BMI ranges on the mechanical milieu of the surgical segment is intricately linked to postoperative disc recurrence. Examining the mechanical shifts in intervertebral discs within lumbar spine surgical segments across different BMI categories carries significant clinical relevance for understanding intervertebral disc degeneration and post-surgical recurrence. Nonetheless, the correlation between different BMI ranges and the postoperative biomechanical alterations of the intervertebral disc remains uncharted territory thus far.

Replicating and assessing the physiological dynamics of the lumbar spine in a live setting is practically unattainable due to existing technological and ethical limitations. Meanwhile, modeling these dynamics in vitro presents significant challenges. Finite Element Analysis (FEA) currently stands as a proficient technique for evaluating biomechanical alterations in the lumbar spine. It possesses the capability to replicate diverse surgical conditions, adjust parameters to generate various models as needed, apply non-destructive force loads, and provide insights into parameters that are not achievable through real-life experiments, such as stress distribution in the annulus fibrosus, nucleus pulposus and endplates [15]. The application of FEA in spinal biomechanics research demonstrates its unique sophistication, particularly in the analysis of spinal imaging data. It offers a highly intuitive digitized portrayal of the biomechanical changes occurring within the spine when subjected to external forces [16,17]. However, there is no reported analysis utilizing finite element analysis to examine postoperative changes in intervertebral disc mechanics among different BMI categories following PETD surgery.

Herein, we conducted simulations to investigate the effects of different BMIs and postures on the stress and deformation of lumbar intervertebral discs in a standard model received L4/5 PETD surgery. Forces of 392 N (BMI 20.76 kg/m^2), 457 N (24.22 kg/m^2), 523 N (27.68 kg/m^2), 588 N (31.14 kg/m^2) and 653 N (34.6 kg/m^2) were applied from the superior edge of the L3 vertebrae. The von Mises stresses and maximum deformation of the L4/5 nucleus pulposus were observed. We hope that the research could offer a theoretical foundation for determining an optimal range of BMI values to be regulated and identifying movements to be avoided in order to minimize disc

recurrence in postoperative patients undergoing PETD surgery.

Materials and methods

Finite element health modeling (L3-S1)

To construct a three-dimensional nonlinear L3-S1 segment, our research team utilized a healthy male subject (30 years old, 170 cm tall, weighing 70 kg) with no prior history of lumbar spine disease, trauma, or surgery. This subject's participation was approved by the Ethics Committee, and they provided informed consent. Utilizing computed tomography (CT) with continuous scanning of subjects, employing a 128-row scanner with a matrix of 512×512, and slice thickness and interval of 0.625 mm, a three-dimensional nonlinear finite element model of the lumbar spine segment from L3 to S1 was established (Fig. 1).

The thin-layer CT scan results of the subjects were imported as DICOM format data into medical imaging software (Mimics 20.0, Belgium Materialise), where the L3-S1 vertebral body model was extracted using threshold segmentation functionality. Subsequent to repairing and erasing commands applied to the cross-sectional images using internal tools in Mimics software, the skeletal outlines of the target structure organization were obtained, followed by running the Calculate 3D function to generate the triangular mesh geometric model of the target structure organization. The geometric model was optimized in Mimics 20.0, exporting a highly accurate triangular mesh STL geometric model with approximate geometric shape, smooth surface, and high-quality triangular mesh. The STL file was imported into Geomagic Wrap 2022 software for surface fitting and smoothing processes, forming a three-dimensional solid geometric model of the lumbar spine L3-S1, where 3-matic (Boolean operation addition and subtraction) was employed to segment the intervertebral discs and vertebral bodies (Fig. 2). After processing, the upper and lower cartilaginous endplates were seamlessly connected to the upper and lower surfaces of the vertebral body.

Through Geomagic Wrap 2022 software, the STL surfaces of each vertebra were separated into 2 mm thickness cortical bone, 1 mm thickness bony endplates (which cover the cortical bone surface of the vertebra and share the same material parameters as cortical bone), and 1 mm thickness cartilaginous endplates. The facet joints are formed by the articulation surfaces of adjacent vertebral bodies, specifically the gap between the inferior facet articulation surface of the superior vertebra and the superior facet articulation surface of the inferior vertebra. The friction coefficient of the facet joints is defined as 0.2. Seven ligaments were simulated using spring elements that only experience tension, including the anterior longitudinal ligament, posterior longitudinal ligament, ligamentum flavum, capsular ligament, interspinous ligament, supraspinous ligament, and intertransverse

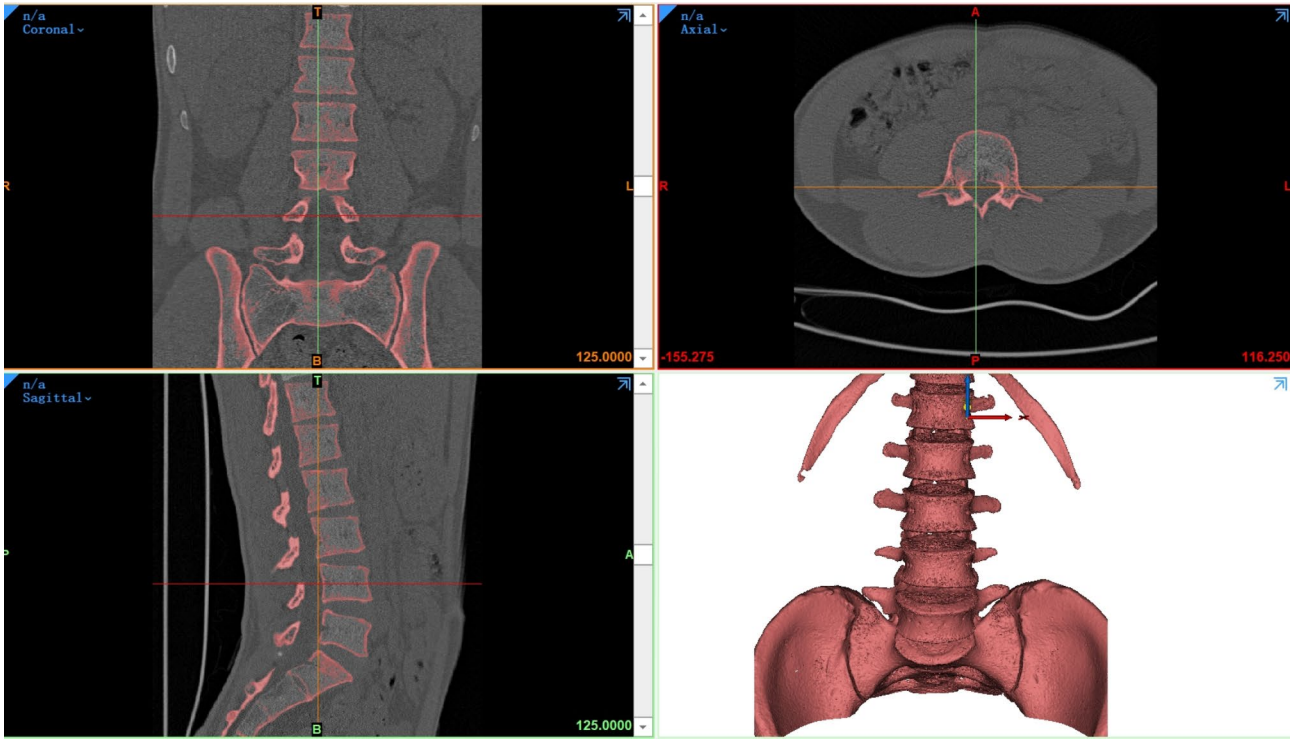

Fig. 1 The volunteer lumbar spine CT image

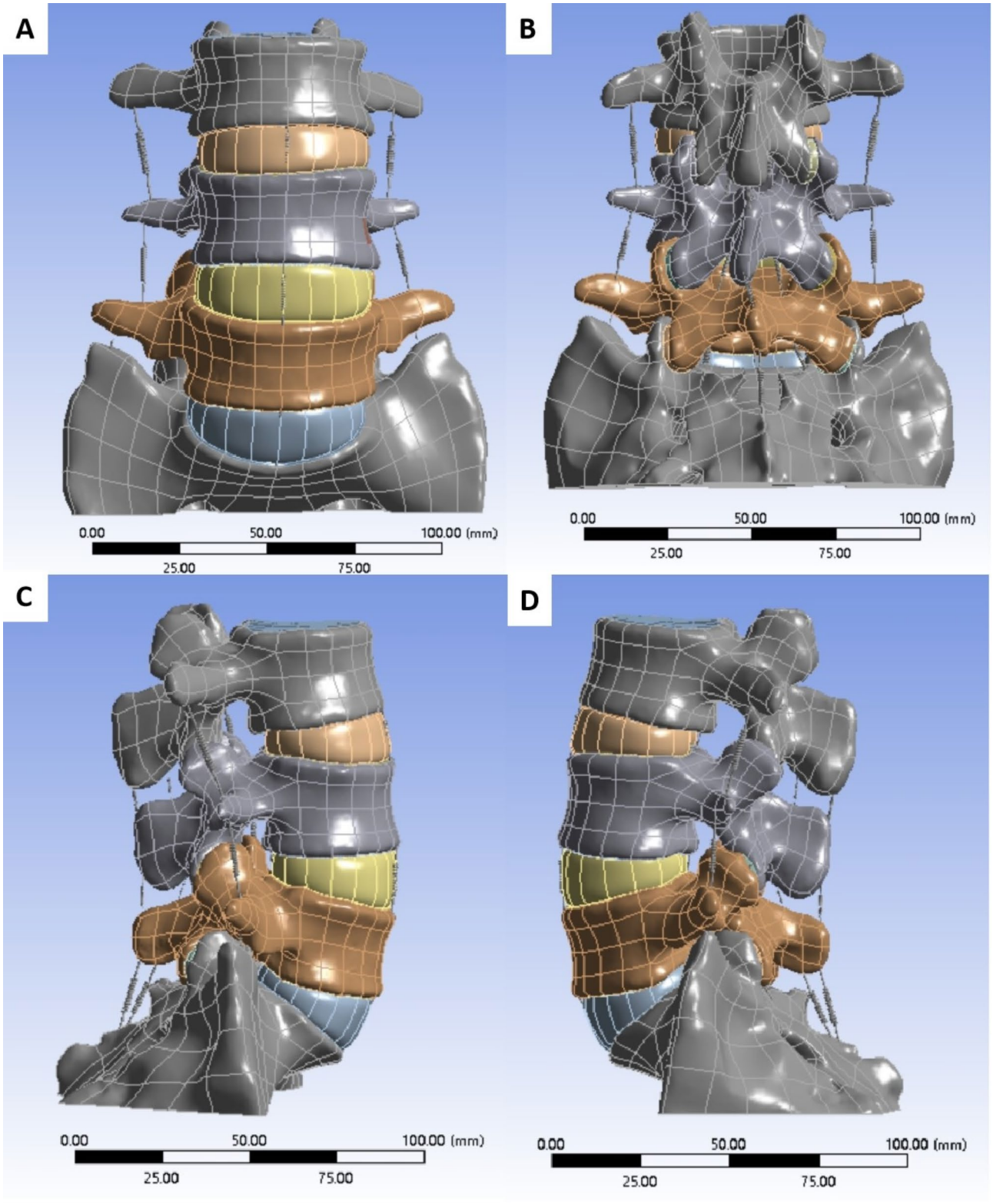

Fig. 2 The lumbar spine three-dimensional model of normal group. The anterior view of the lumbar spine three-dimensional model (**A**); The back view of the lumbar spine three-dimensional model (**B**); The right lateral view of the lumbar spine three-dimensional model (**C**); The left lateral view of the lumbar spine three-dimensional model (**D**)

ligament [18]. Finally, finite element model parameters were defined. The normal bone density normal group (NG) consisted of a total of 187,590 elements and 240,307 nodes, while the normal bone density PETD surgery group (PETDSG) comprised a total of 223,653 elements and 272,533 nodes. The material properties of the L3-S1 spinal functional unit are presented in Table 1 [19–21].

Establishment of finite element PELD surgical model (L3-S1)

In Autodesk Inventor software, surgical procedures are simulated from the tip of the superior articular process to the posterior superior margin of the vertebral body (Zone), with a simulated outer diameter of 7.5 mm for the ring saw cutting of the superior articular process (Figure 3). Concurrently, the simulation involves the surgical excision of a portion of the annulus fibrosus and nucleus pulposus, removing the right posterior annulus fibrosus and nucleus pulposus of the L4/5 intervertebral disc, measuring 17.5 mm in length, 3 mm in width, and 5 mm in height (Fig. 4). Finite element analysis and biomechanical analysis of the three-dimensional finite element model are conducted using ANSYS 15.0 software.

Material properties, boundaries, and loading conditions on the boundaries of finite element structural models

Assumptions for constraints: (1) Fixed constraints are applied to the bottom end of the S1 vertebra, restricting six degrees of freedom; (2) Assumptions are made regarding the isotropic, homogeneous, and continuous linear elastic properties of the vertebrae, bony endplates, cartilaginous endplates, etc. The annulus fibrosus and nucleus pulposus are considered hyperelastic materials. Ligaments are simplified as nonlinear spring elements subjected only to tension, representing a position-dependent plastic material; (3) During model validation, a vertical load of 500 N (equivalent to 2/3 of body weight, representing axial compression on the lumbar vertebrae in an upright posture) is uniformly applied to the upper surface of the L3 vertebra in a normal lumbar spine model (L3-S1). Additionally, a moment of 10 N•m is applied to the upper surface of L3 to simulate various biomechanical properties of the lumbar spine under conditions such as upright posture, flexion, extension, lateral bending, and rotation. (4) With a patient height of 1.7 m, simulations are conducted for patients weighing 60 kg, 70 kg, 80 kg, 90 kg, and 100 kg, calculated as 2/3 of body weight. Loads are distributed on the upper surface of L3 as 392 N, 457 N, 523 N, 588 N, and 653 N, respectively, resulting in BMIs of 20.76 kg/m^2, 24.22 kg/m^2, 27.68 kg/m^2, 31.14 kg/m^2 and 34.6 kg/m^2. Simulations mimic normal lumbar spine activity in both normal individuals and postoperative patients, with fixed constraints applied to the bottom end of the S1 vertebra, under seven conditions: upright posture, flexion, extension, lateral bending, and rotation, each limited to 3°.

Table 1 Material properties of the L3-S1 finite element model

Tissue	Young's modulus (MPa)	Poisson's ratio
Cortical bone	12 000	0.3
Cancellous bone	100	0.2
cartilaginous endplate	1000	0.4
Cortical endplate	12 000	0.3
Annular collagen fiber	360–550	0.3
Annular ground substance	Hyperelastic C1 = 0.18, C2 = 0.045	
Nucleus pulposus	Hyperelastic C1 = 0.12, C2 = 0.030	
Posterior element	3 500	0.25

Observation indicators

The equivalent von Mises stresses and maximum deformation of the L4/5 nucleus pulposus in both normal group and PETD surgery group with different BMIs are observed. Additionally, alterations in the location and size of the high stress concentration area within the stress cloud map were also observed.

Results

Model validation

The present study has successfully established a non-destructive finite element model of the normal L3-S1 lumbar spine segment, simulating the three-dimensional structure of cortical bone, trabecular bone, intervertebral discs, and associated ligaments, totaling 187,590 elements and 240,307 nodes. To validate the modeling approach, proper setup, boundary conditions, and assumptions, this study conducted biomechanical simulations of flexion, extension, lateral bending, and rotation on the normal L3-S1 lumbar spine model under identical loads and constraints. Through qualitative and quantitative analyses, the study found that the range of motion data obtained were consistent with previous studies in trend and numerical values [22]. The established model proved effective, possessing a well-defined geometry and high-fidelity simulation, thereby suitable for relevant biomechanical research and analysis. Validation of Model Efficacy was illustrated in Table 2.

3.2 Variations in stress distribution across different BMIs and movement types between the normal group and PETD surgical group.

L4/5 NP equivalent von mises stress

As illustrated in Fig. 5, the equivalent von Mises stress in the L4/5 NP was observed to escalate with different BMI values in both the NG and PETDSG cohorts. In the absence of motion, during anterior flexion and posterior

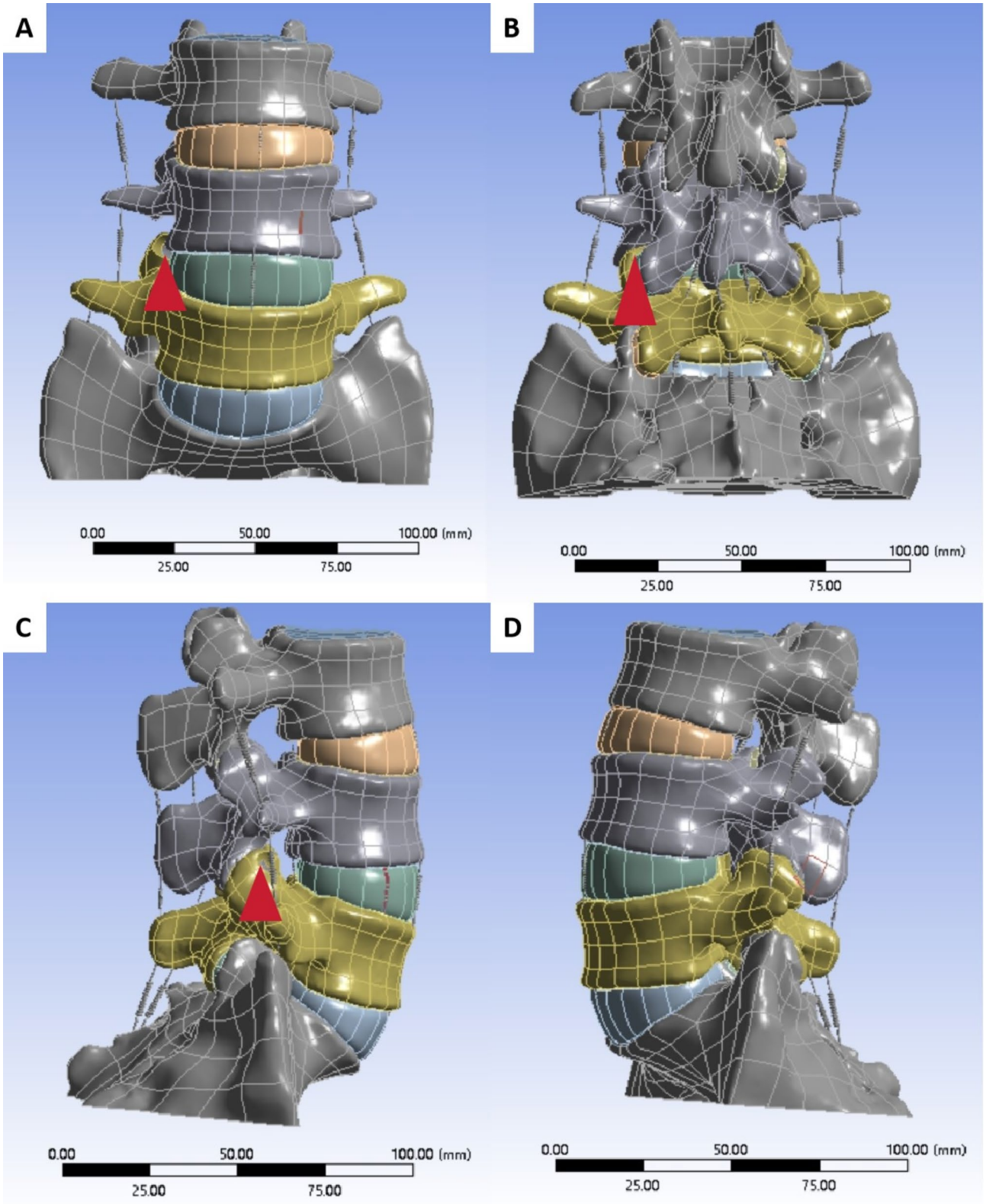

Fig. 3 The lumbar spine three-dimensional model of PETD surgery group. The anterior view of the lumbar spine three-dimensional model (**A**); The back view of the lumbar spine three-dimensional model (**B**); The right lateral view of the lumbar spine three-dimensional model (**C**); The left lateral view of the lumbar spine three-dimensional model (**D**). Resected superior articular process indicated by The red triangle indicated the resected superior facet joint

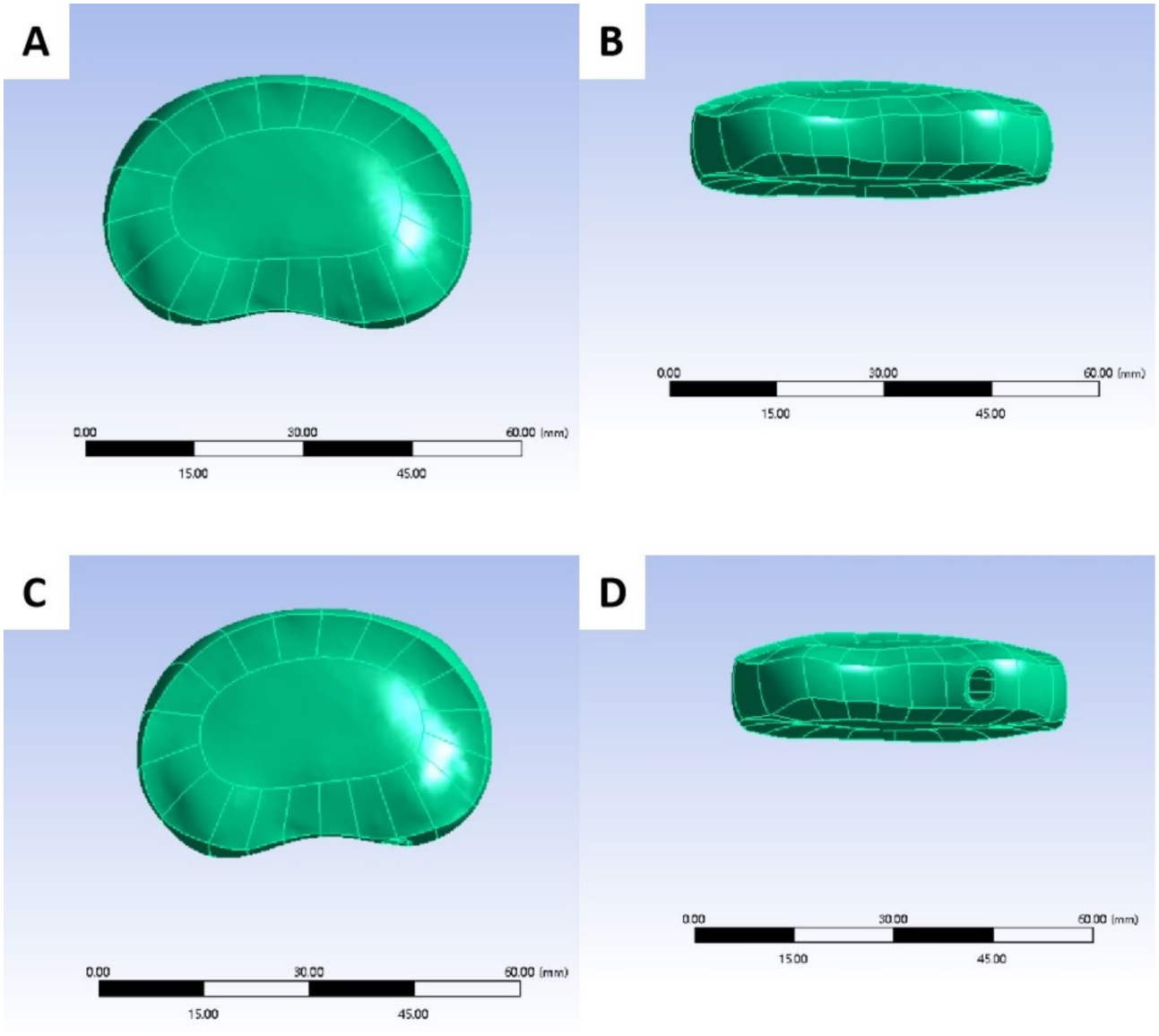

Fig. 4 The intervertebral disc model. The superior view (**A**) and posterior view (**B**) of intervertebral disc in normal group. The superior view (**C**) and posterior view (**D**) of intervertebral disc in PETD surgery group

Table 2 Validation of model validity

	Present study			Yamamoto I et al.			Xiao Z et al.		
	Flexion and Extension	Bending	Rotation	Flexion and Extension	Bending	Rotation	Flexion and Extension	Bending	Rotation
L3-L4	11.02	12.15	5.6	11.3 ± 1.70	12.2 ± 1.70	5.1 ± 1.38	11.78	13.2	5.76
L4-L5	13.46	12.16	4.99	14.8 ± 2.10	12.2 ± 2.25	3.7 ± 1.50	14.2	13.23	4.23
L5-S1	15.69	11.48	2.89	16.9 ± 2.05	11.3 ± 2.35	2.5 ± 0.75	17.29	12.56	2.7

extension: It was noted that the L4/5 NP equivalent von Mises stresses were most pronounced in the anterior flexion posture and least in the static position (Fig. 5A-B). In the normal group, the overall von Mises stresses at the L4/5 NP generally exhibited lower values during right lateral bending compared to left bending. However, in the PETD surgery group, the stresses during right lateral bending were higher than during left bending, with a statistically significant and notably greater increase observed during right bending compared to left bending (Fig. 5C-D). Besides, in the normal group, the overall von Mises stresses at the L4/5 NP showed a greater magnitude during left rotation compared to right rotation, while in the PETD surgery group, not only were the stresses greater during left rotation compared to right rotation, but also the magnitude of increase during left

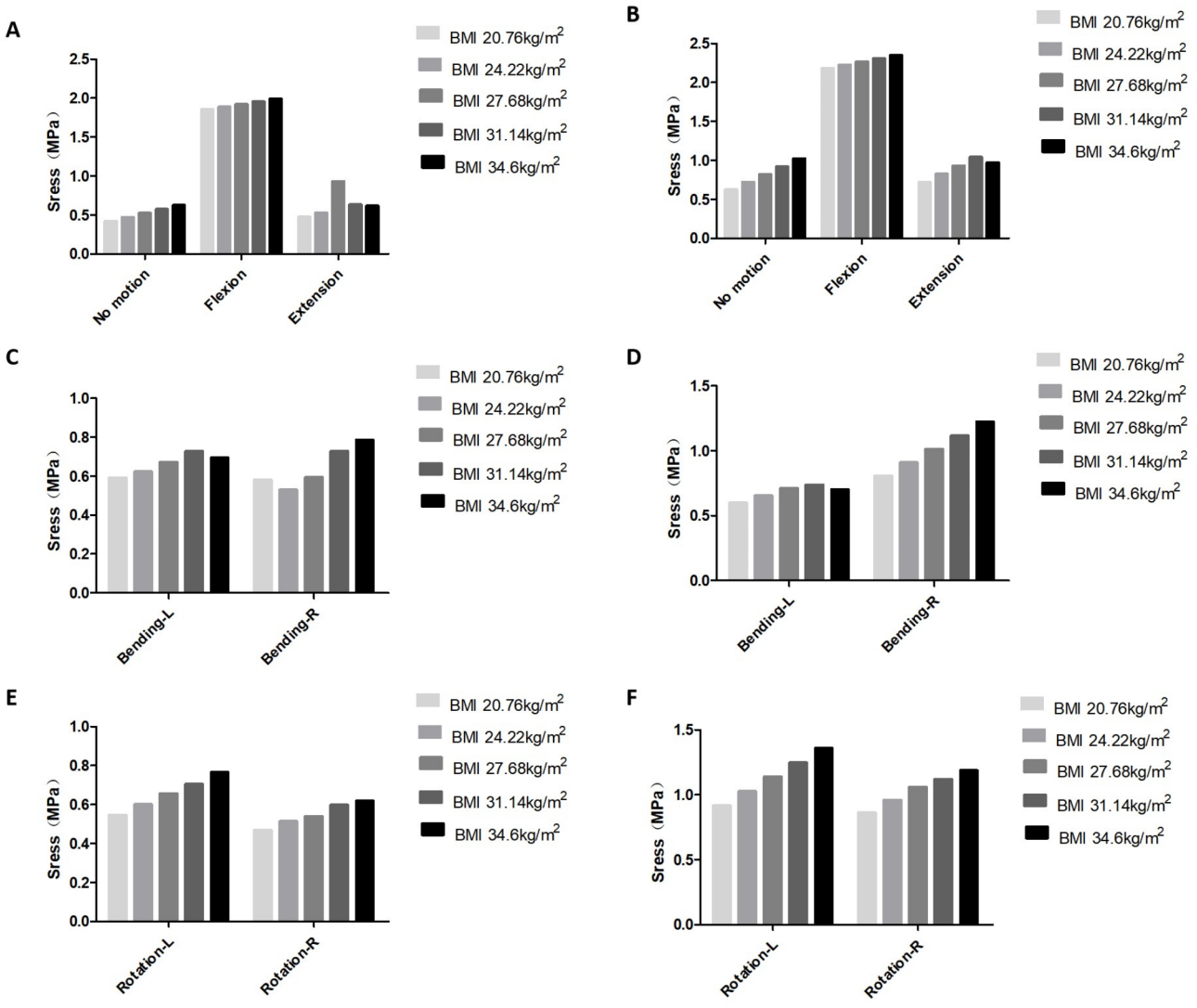

Fig. 5 L4/5 NP equivalent von mises stress with different BMI values in different motions in both the normal group and PETD surgery group. L4/5 NP von mises stress with different BMI values in no motion, flexion and extension in normal group (**A**) and PETD surgery group (**B**); L4/5 NP von mises stress with different BMI values in Bending-L and Bending-R in normal group (**C**) and PETD surgery group (**D**); L4/5 NP von mises stress with different BMI values in Rotation-L and Rotation-R in normal group (**E**) and PETD surgery group (**F**)

rotation was notably larger than during right rotation (Fig. 5E-F).

Maximum deformation of L4/5 NP

Among the no motion, flexion and extension movement, the maximum deformation of the L4/5 NP increased with higher BMI, with the largest deformation occurring in forward bending and the smallest in backward extension in both the control group and the PETD surgery group (Fig. 6A-B). As for the lateral bending movement, with increasing BMI, the maximum deformation of the L4/5 NP in both the normal group and PETD surgery group initially showed smaller values in right lateral bending compared to left bending. However, when BMI reached 34.6 kg/m^2, the deformation in the right bending position exceeded that in the left bending position (Fig. 6C-D). In the left and right rotation movement, the deformation of the L4/5 NP was consistently smaller in right rotation than in left rotation under the same BMI and model condition (Fig. 6E-F).

NP stress distribution in NG and PETDSGs at different BMIs and motions

Increasing BMI was found to lead to an increase in high-stress areas and locations on the compressed side of the L4/5 nucleus pulposus during flexion (Fig. 7), extension (Fig. 8), left bending (Fig. 9) and right bending (Fig. 10). In the context of left rotation, the region with the highest stress on the left side of both groups of nucleus pulposus exhibited an increase in area as BMI increased (Fig. 11).

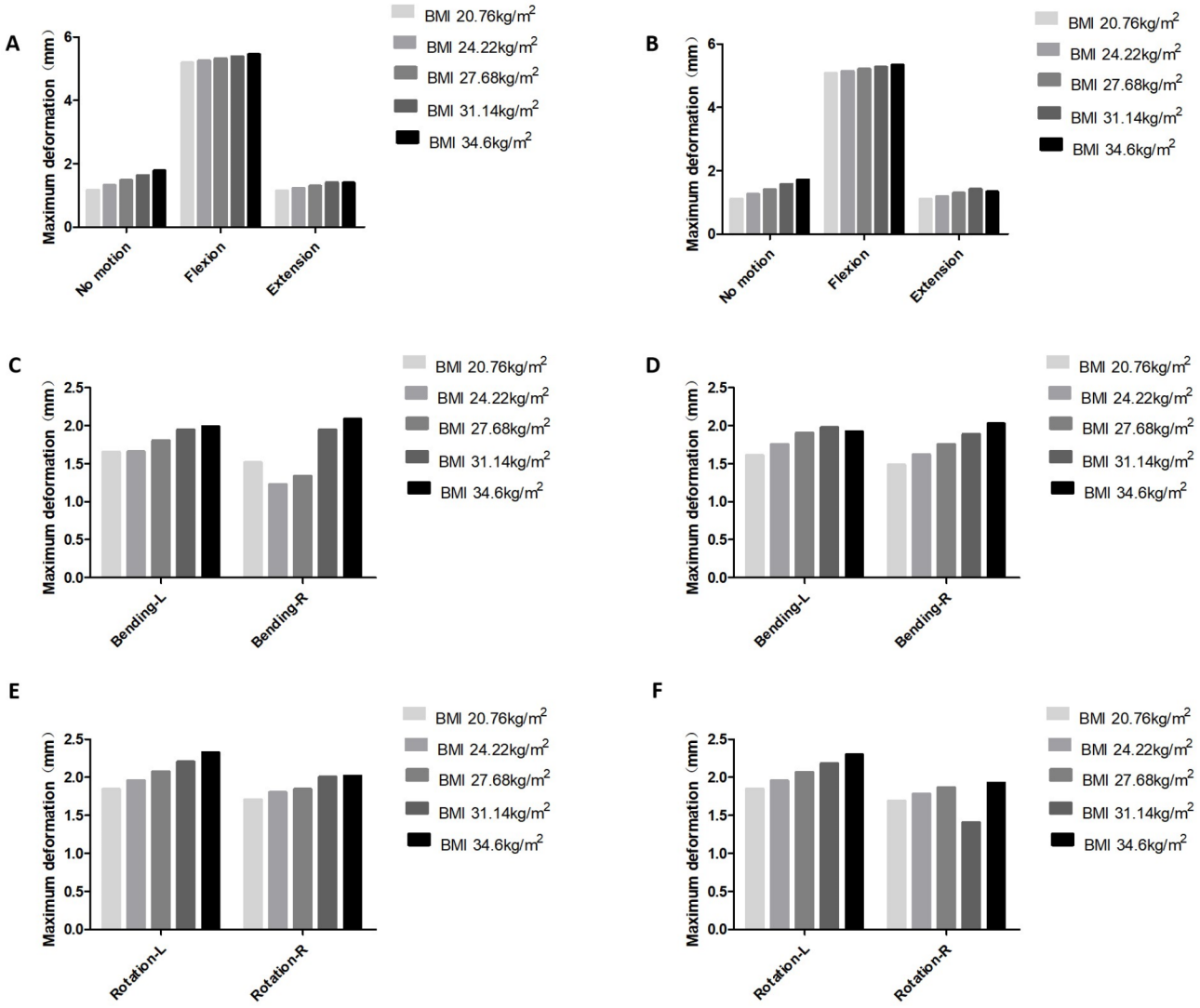

Fig. 6 Maximum deformation of L4/5 NP with different BMI values in different motions in both the normal group and PETD surgery group. Maximum deformation of L4/5 NP with different BMI values in no motion, flexion and extension in normal group (**A**) and PETD surgery group (**B**); Maximum deformation of L4/5 NP with different BMI values in Bending-L and Bending-R in normal group (**C**) and PETD surgery group (**D**); Maximum deformation of L4/5 NP with different BMI values in Rotation-L and Rotation-R in normal group (**E**) and PETD surgery group (**F**)

Conversely, in right rotation, the area of the highest stress region in both groups of NP increased, albeit with a position change closer to the periphery (Fig. 12). In the absence of movement, the area of the highest stress region in both groups of the NP and the highest stress region experienced an increase, with the highest stress region expanding from posterior to anterior and from external to internal (Fig. 13). Notably, in the area where NP were damaged, conspicuous high stress areas were observed, indicating a concentration of stress.

Discussion

Endoscopic spine surgery is currently the most popular minimally invasive decompression surgery for treating lumbar disc herniation [23]. Previous studies have indicated that LDH patients who undergo surgery generally experience significant clinical improvement. However, a portion of LDH patients who undergo surgery still face the risk of postoperative recurrence [24,25]. It has been reported that the incidence rates of recurrence and reoperation after PETD are 6.3% (4-10%) and 3.66% (2.33-4.8%), respectively, which impose a significant burden on both patients and their families [26]. Therefore, identifying the primary factors leading to postoperative recurrence of LDH and implementing targeted treatment or preventive measures can reduce the recurrence rate of LDH treated with PETD. The majority of scholars concur that age and BMI are independent risk factors for postoperative disc recurrence [27,28]. Besides, *Ren et al.* [29] analyzed 1,159 patients who underwent percutaneous

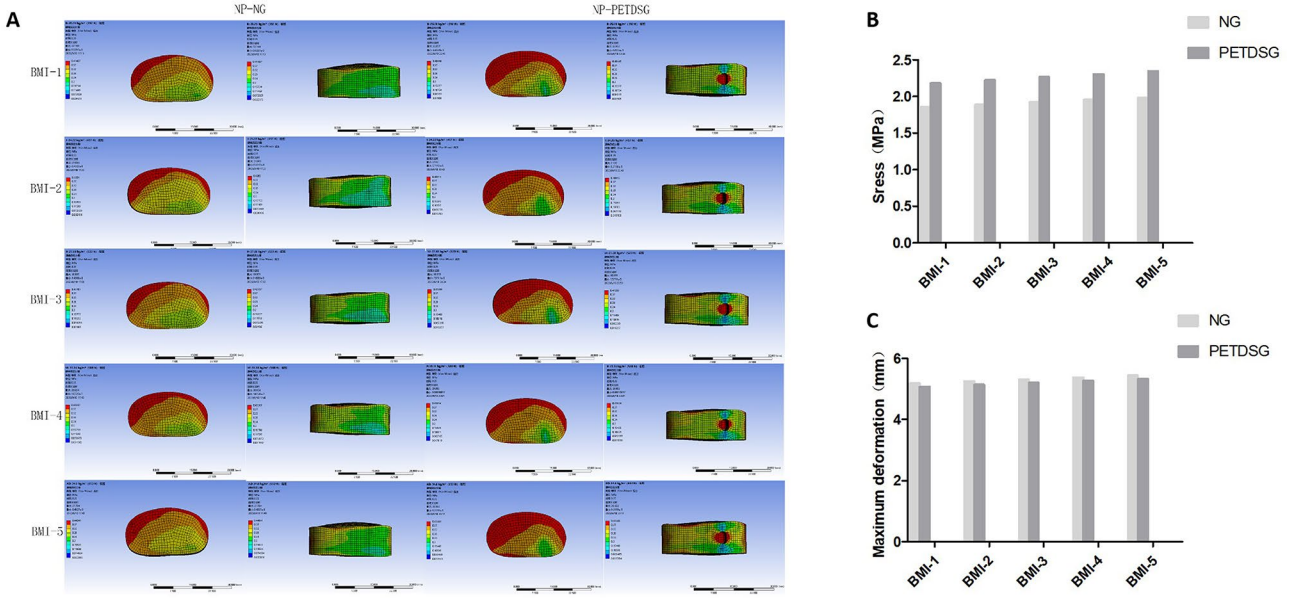

Fig. 7 The impact of flexion on the stress distribution within the NP, revealing a noteworthy disparity between the left anterior red stress area of the PETDSG and that of the NG (**A**). L4/5 NP equivalent von mises stress with different BMIs in flexion in the normal group and PETD surgery group (**B**). Maximum deformation of L4/5 NP with different BMIs in flexion in the normal group and PETD surgery group (**C**). BMI-1 20.76 kg/m^2、BMI-2 24.22 kg/m^2、BMI-3 27.68 kg/m^2、BMI-4 31.14 kg/m^2、BMI-5 34.6 kg/m^2

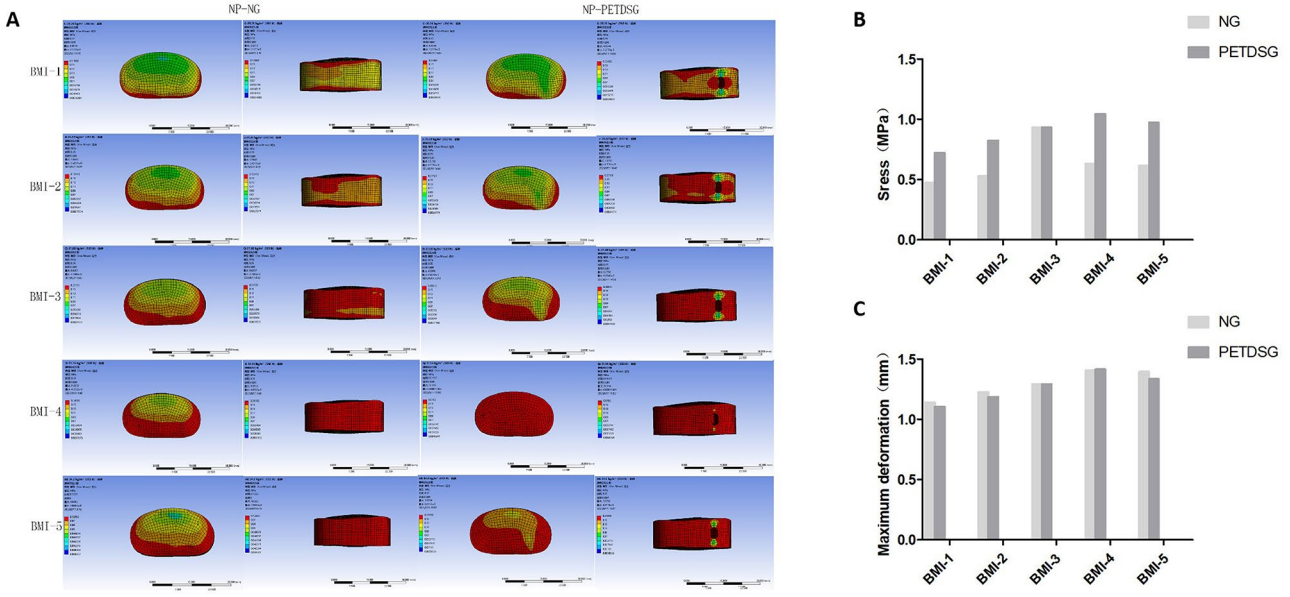

Fig. 8 The alteration in the stress distribution within the NP under posterior extension (**A**). L4/5 NP equivalent von mises stress with different BMIs in extension in the normal group and PETD surgery group (**B**). Maximum deformation of L4/5 NP with different BMIs in extension in the normal group and PETD surgery group (**C**). BMI-1 20.76 kg/m^2、BMI-2 24.22 kg/m^2、BMI-3 27.68 kg/m^2、BMI-4 31.14 kg/m^2、BMI-5 34.6 kg/m^2

endoscopic lumbar discectomy and identified BMI as a risk factor for predicting recurrence of lumbar disc surgery. *Dobran et al.* [30]. also indicated a significant correlation between higher BMI and postoperative recurrence of LDH. During clinical surgery, the protruding nucleus pulposus can be obscured by the superior articular process, hence partial resection of the superior articular process is necessary when removing the protruding nucleus pulposus. *Lawrence et al.* [31] developed the MSU disc typology, which classifies disc herniation based on its location and severity on MRI scans. A perpendicular line is delineated at the inner edge of the facet joint on both sides, subsequently divided into four equal segments. In cases where a sizable herniated disc is situated

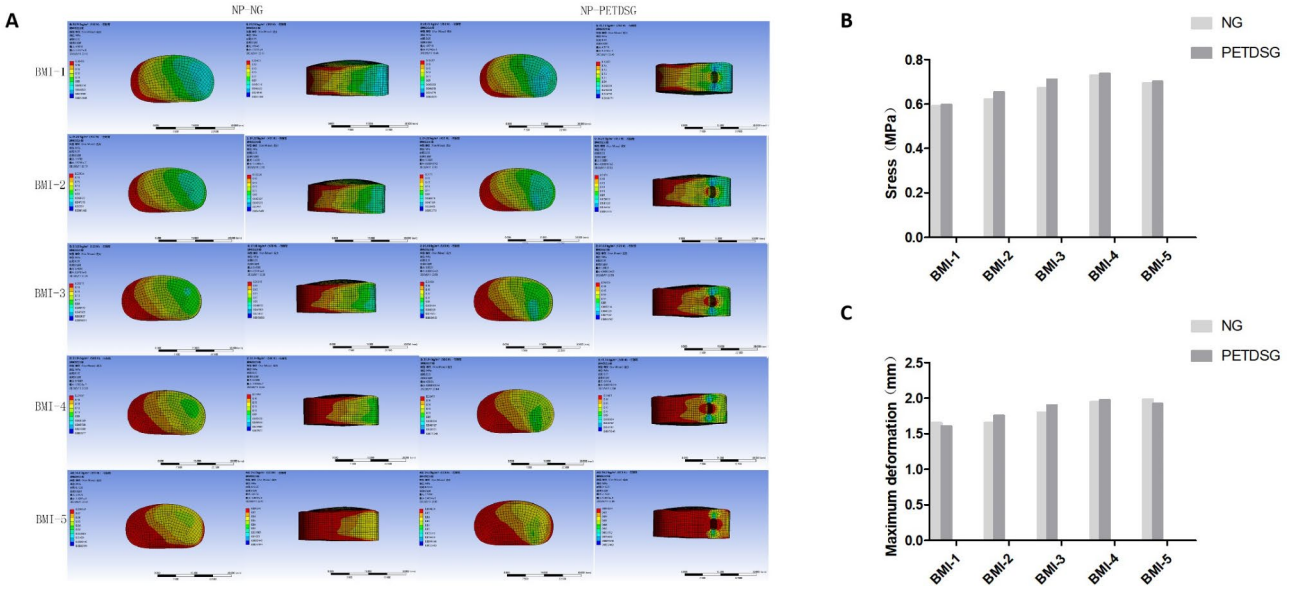

Fig. 9 The alteration of the stress cloud map in Bending-L condition (**A**). L4/5 NP equivalent von mises stress with different BMIs in Bending-L in the normal group and PETD surgery group (**B**). Maximum deformation of L4/5 NP with different BMIs in Bending-L in the normal group and PETD surgery group (**C**). BMI-1 20.76 kg/m^2、BMI-2 24.22 kg/m^2、BMI-3 27.68 kg/m^2、BMI-4 31.14 kg/m^2、BMI-5 34.6 kg/m^2

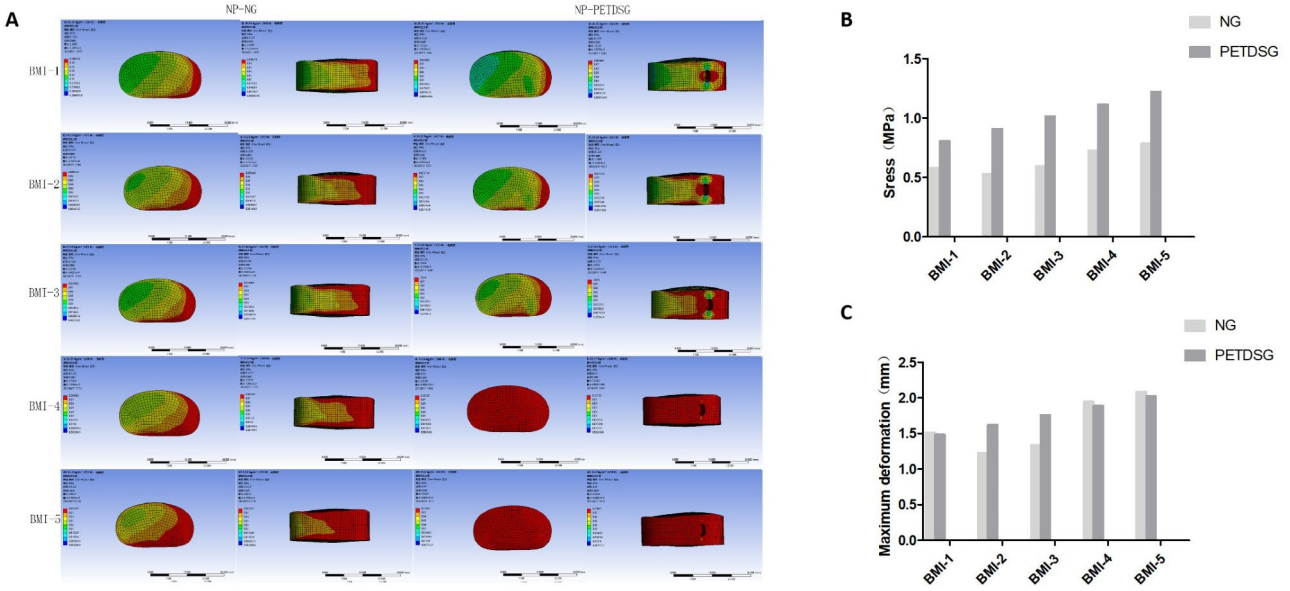

Fig. 10 The alteration of the stress distribution within the NP under Bending-R (**A**). L4/5 NP equivalent von mises stress with different BMIs in Bending-R in the normal group and PETD surgery group (**B**). Maximum deformation of L4/5 NP with different BMIs in Bending-R in the normal group and PETD surgery group (**C**). BMI-1 20.76 kg/m^2、BMI-2 24.22 kg/m^2、BMI-3 27.68 kg/m^2、BMI-4 31.14 kg/m^2、BMI-5 34.6 kg/m^2

in the central region, it is more likely to result in cauda equina syndrome, rendering minimally invasive surgical alternatives less optimal. Conversely, for highly lateral or foraminal disc herniations, there is no necessity to contour the facet joint. The posterior longitudinal ligament exhibits increased thickness and occupies a central anatomical position. The NP commonly protrudes in proximity to this ligament, particularly in zone II. Hence, we delineated the surgical trajectory from the apex of the right superior articular eminence to the posterior aspect of the disc within zone II in this study. We simulated the utilization of a 7.5-mm annular saw during endoscopy to contour the superior articular eminence, followed by partial excision of the NP.

In the PETD surgery group, both von Mises stress and the maximum deformation of the NP show a gradual increase as BMI increases. Furthermore, the von Mises stress and maximum deformation of the NP in flexion

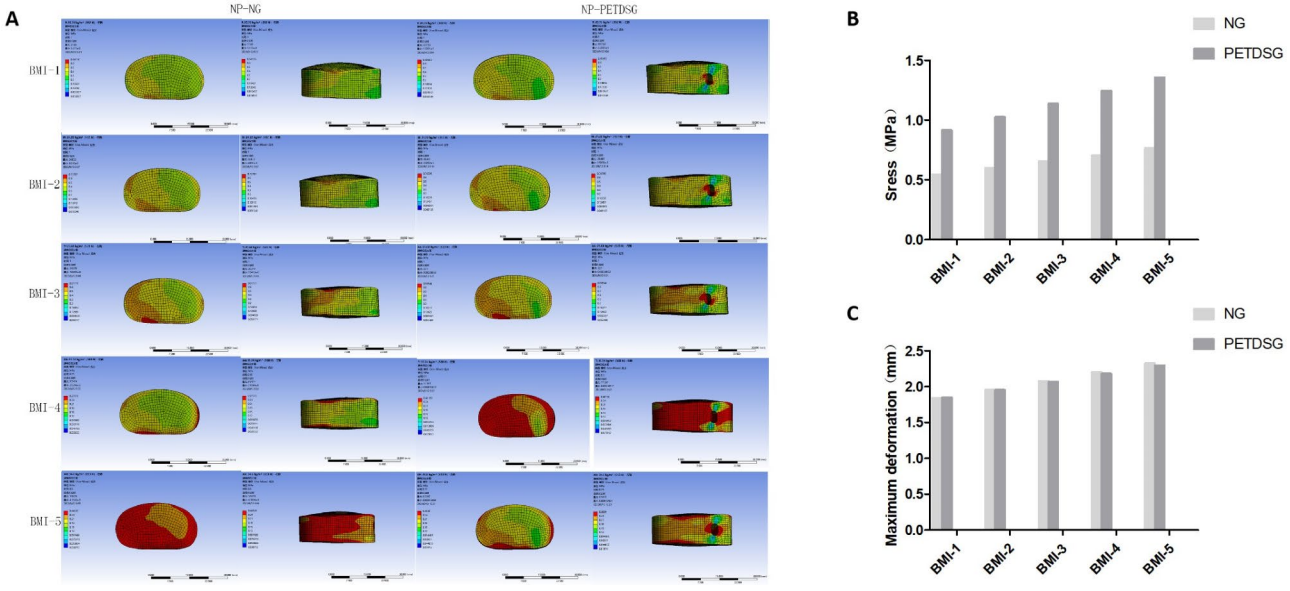

Fig. 11 The impact of Rotation-L on the alteration of the stress cloud map in the NP (**A**). L4/5 NP equivalent von mises stress with different BMIs in Rotation-L in the normal group and PETD surgery group (**B**). Maximum deformation of L4/5 NP with different BMIs in Rotation-L in the normal group and PETD surgery group (**C**). BMI-1 20.76 kg/m^2、BMI-2 24.22 kg/m^2、BMI-3 27.68 kg/m^2、BMI-4 31.14 kg/m^2、BMI-5 34.6 kg/m^2

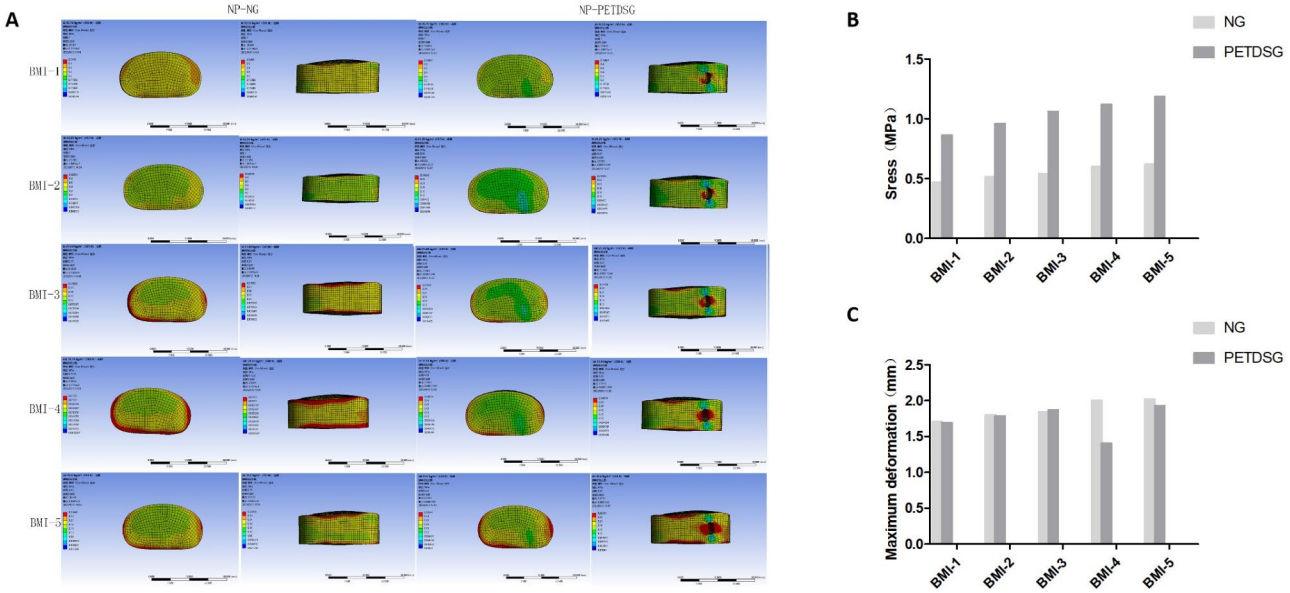

Fig. 12 The impact of Rotation-R on the NP stress cloud map (**A**). L4/5 NP equivalent von mises stress with different BMIs in Rotation-R in the normal group and PETD surgery group (**B**). Maximum deformation of L4/5 NP with different BMIs in Rotation-R in the normal group and PETD surgery group (**C**). BMI-1 20.76 kg/m^2、BMI-2 24.22 kg/m^2、BMI-3 27.68 kg/m^2、BMI-4 31.14 kg/m^2、BMI-5 34.6 kg/m^2

loading are significantly higher than in other loading conditions under the same BMI condition. Therefore, it is advisable for patients to reduce flexion movements post-surgery. Besides, the von Mises stresses at the L4/5 NP are greater during right lateral bending compared to left bending. We hypothesize that the significant compensatory increase in von Mises stresses during right bending is attributable to the partial resection of the right superior articular process. We considered that with increasing body weight, there is a notable enlargement in the stress concentration area of the nucleus pulposus, resulting in an increase in von Mises stresses, and a significantly elevated likelihood of recurrent nucleus pulposus injury. Therefore, postoperative obese patients should endeavor to avoid flexion movements towards the operated side as much as possible.

As shown in Figs. 7, 8, 9, 10, 11, 12 and 13, the results indicated that both von Mises stress and the maximum

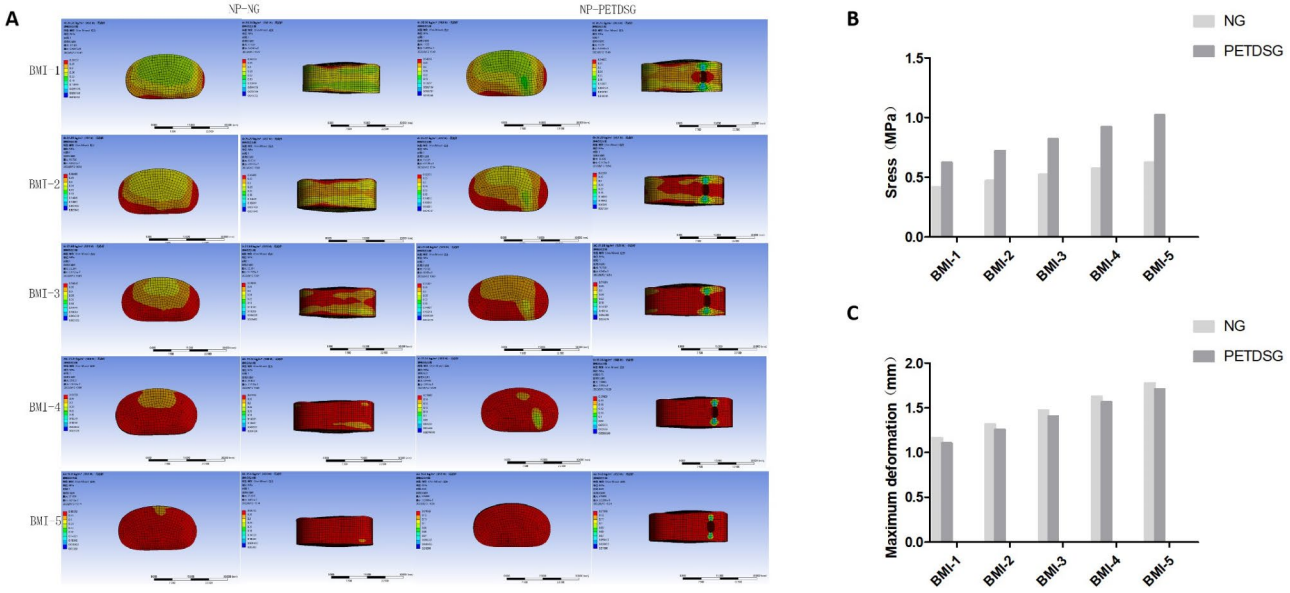

Fig. 13 The NP stress cloud map of no motion (**A**). L4/5 NP equivalent von mises stress with different BMIs in no motion in the normal group and PETD surgery group (**B**). Maximum deformation of L4/5 NP with different BMIs in no motion in the normal group and PETD surgery group (**C**). BMI-1 20.76 kg/m^2、BMI-2 24.22 kg/m^2、BMI-3 27.68 kg/m^2、BMI-4 31.14 kg/m^2、BMI-5 34.6 kg/m^2

deformation of the medulla in the PETD-SG group are higher than those in the NG group under the same BMI conditions except for the left flexion condition. This suggests that the postoperative biomechanical environment of the lumbar spine is significantly affected by the PETD facet joint shaping procedure, consistent with previous research findings [32].Therefore, it suggested that surgeons should strive for precise shaping when removing facet joints during surgery to avoid unnecessary facet joint injury, which could lead to lumbar spine instability. From the stress distribution maps, we observed that with increasing BMI, the area of high stress in the nucleus pulposus continuously increases, with localized stress concentration in certain areas and a gradual increase in nuclear stress, indicating that high BMI may predispose to intervertebral disc recurrence. Previous studies have indicated that, with the periodic increase in pressure within the intervertebral disc, overweight conditions may lead to higher shear strains in the outer posterior portion of the annulus fibrosus, resulting in disc protrusion, consistent with the findings of this study [33,34].

The von Mises stress and the maximum deformation of the lumbar intervertebral disc in the PETD-SG group exhibited an increase across all seven directional angles with the rise in BMI. It is advisable for patients to remain bedridden in the early stages, and if ambulation is required, the utilization of a waist belt or brace for protection is recommended in clinic. Our study substantiates the theoretical underpinnings for the recommendation. Patients afflicted with lumbar disc herniation frequently exhibit paraspinal muscle fat infiltration, and the severity of the infiltration correlates with the accelerated progression of lumbar disc herniation, indicating that paraspinal muscle fat infiltration constitutes one of the risk factors for lumbar disc herniation [35,36]. For patients with elevated BMI and concurrent paraspinal muscle fat infiltration, it is advisable to reduce BMI both preoperatively and postoperatively, while concurrently enhancing the functionality of the lumbodorsal muscles. During the periods of bed rest, although gravitational forces are mitigated, rotational shear forces may persist. This implies that when patients after PETD surgery engage in lumbodorsal muscle exercises, it is crucial to minimize lumbar rotation movements, as it could prove more advantageous for the recovery of the intervertebral disc after surgery.

Our study has several limitations. Firstly, the geometric model used in this study can simulate various materials and loading methods. However, it does not take into account the influence of soft tissues, such as living muscles and intervertebral disc degeneration on spinal stability. Besides, The investigation does not consider the sex-related variations in fat.

distribution across different BMI categories. Secondly, due to individual differences in the human body, the finite element model cannot fully represent the real situation for all individuals, nor can it completely simulate actual surgical scenarios. Nevertheless, advancements in computer technology are expected to progressively enhance the fidelity of finite element models towards real-world conditions. In clinical practice, while conducting PETD surgery and facet joint modeling, we observed

significant distinctions between young and old patients. The majority of the old patients suffer from osteoporosis, rendering the modeling process relatively straightforward, whereas young patients possess denser bones, which made the procedure complicated. For osteoporotic patients, it is essential to explore whether the stress and deformation characteristics of the intervertebral disc under varying BMIs exhibit similar patterns to those observed in non-osteoporotic patients. To this end, we have developed normal and surgical finite element models for osteoporotic patients and compared the stress and deformation changes across different BMI categories. We anticipate that the insights derived from this research will contribute to the formulation of superior clinical recommendations for this specific patient cohort. We will also investigate the impact of factors such as fatty infiltration, disc degeneration and vertebral curvature on the stress and deformation of intervertebral discs following PETD surgery in patients with varying BMIs in the future study.

Conclusion

Through finite element analysis and without considering the fatty infiltration of paravertebral muscles, this research simulates the alterations in stress and deformation of lumbar intervertebral discs in the same patient at different BMIs and postures, it was found that higher BMI is more likely to increase the equivalent von Mises stress on the nucleus pulposus, resulting in a significant enlargement of the high-stress area, and a distinct concentration of stress in the surgical impact zones of the NP, indicating that patients recovering from PETD surgery should refrain from overly strenuous activities during early rehabilitation, and also advises that patients with high BMI should aim for a scientific weight reduction before and after surgery, as maintaining suitable stress levels on the intervertebral disc tissue could be conducive to its self-repair.

Acknowledgements
Not applicable.

Author contributions
The experimental design was executed by Xiaohai Zhang and Zongsheng Yin, while the implementation of the experiment was conducted by Xiaohai Zhang and Jinghui Lin. Xiaohai Zhang, Chen Liu, Shuangtao Xue and Mengying Wu took on the responsibility of writing the manuscript. Zongsheng Yin was in charge of proofreading and editing.

Funding
This study was supported by funding from the National Natural Science Foundation of China (82172427); National Natural Science Foundation of Anhui Province (1708085QH205); Excellent Young Project of Anhui Provincial University Research Project (2023AH030104).

Data availability
No datasets were generated or analysed during the current study.

Declarations

Ethics approval and consent to participate
Our study was approved by the Ethics Committee of The Second People's Hospital of Wuhu City (Approval: 2024-KY-003). All methods were carried out in accordance with relevant guidelines and regulations.

Consent for publication
Not applicable.

Competing interests
The authors declare no competing interests.

Author details
[1]Department of Orthopaedics, The First Affiliated Hospital of Anhui Medical University, Hefei, Anhui 230032, China
[2]The Second People's Hospital of Wuhu City, Wuhu, Anhui 241001, China
[3]Wuhu Institute of Technology, Wuhu, Anhui 241000, China
[4]Department of Spine Surgery, Yijishan Hospital of Wannan Medical College, Wuhu, Anhui 241001, China

Received: 11 September 2024 / Accepted: 25 November 2024
Published online: 26 December 2024

References

1. Hoy D, Bain C, Williams G, March L, Brooks P, Blyth F, et al. A systematic review of the global prevalence of low back pain. Arthritis Rheum. 2012;64(6):2028–37.
2. Fatoye F, Gebrye T, Odeyemi I. Real-world incidence and prevalence of low back pain using routinely collected data. Rheumatol Int. 2019;39(4):619–26.
3. Kreiner DS, Hwang SW, Easa JE, Resnick DK, Baisden JL, Bess S. ea al. An evidence-based clinical guideline for the diagnosis and treatment of lumbar disc herniation with radiculopathy. Spine J. 2014;14(1):180 – 91.
4. Wang K, Wen HN, Song M. Special clinical phenomena: Nucleus Pulposus re-absorption of L5-S1 giant disc herniation. Asian J Surg. 2023;46(4):1710–11.
5. Li HY, Jiang CQ, Mu XS, Lan WR, Zhou Y, Li CQ. Comparison of MED and PELD in the treatment of adolescent lumbar disc herniation: a 5-Year retrospective Follow-Up. World Neurosurg. 2018;112:e255–60.
6. Chen Z, Zhang LM, Dong JW, Xie P, Liu B, Wang Q, et al. Percutaneous transforaminal endoscopic discectomy compared with microendoscopic discectomy for lumbar disc herniation: 1-year results of an ongoing randomized controlled trial. J Neurosurg Spine. 2018;28(3):300–10.
7. Suk KS, Lee HM, Moon SH, Kim NH. Recurrent lumbar disc herniation: results of operative management. Spine (Phila Pa 1976). 2001;26(6):672–6.
8. Lee JH, Choi KC, Lee JH. Could the splitting of the Annulus during Percutaneous endoscopic lumbar diskectomy (PELD) be a culprit for recurrent disk herniation? An analysis of the Reherniation Pattern after PELD. World Neurosurg. 2019;132:e623–9.
9. Siccoli A, Schröder ML, Staartjes VE. Association of age with incidence and timing of recurrence after microdiscectomy for lumbar disc herniation. Eur Spine J. 2021;30(4):893–8.
10. Yin S, Du H, Yang WZ, Duan CG, Feng CS, Tao HR. Prevalence of recurrent herniation following percutaneous endoscopic lumbar discectomy: a Meta-analysis. Pain Physician. 2018;21(4):337–50.
11. Meredith DS, Huang RC, Nguyen J, Lyman S. Obesity increases the risk of recurrent herniated nucleus pulposus after lumbar microdiscectomy. Spine J. 2010;10(7):575–80.
12. Park CH, Park ES, Lee SH, Lee KK, Kwon YK, Kang MS, et al. Risk factors for early recurrence after Transforaminal endoscopic lumbar disc decompression. Pain Physician. 2019;22(2):E133–8.
13. Siccoli A, Staartjes VE, Klukowska AM, Muizelaar JP, Schröder ML. Overweight and smoking promote recurrent lumbar disk herniation after discectomy. Eur Spine J. 2022;31(3):604–13.
14. Luo MJ, Wang ZZ, Zhou BJ, Yang GG, Shi YX, Chen J, et al. Risk factors for lumbar disc herniation recurrence after percutaneous endoscopic lumbar discectomy: a meta-analysis of 58 cohort studies. Neurosurg Rev. 2023;46(1):159.
15. Du CF, Cai XY, Gui W, Sun MS, Liu ZX, Liu CJ, et al. Does oblique lumbar interbody fusion promote adjacent degeneration in degenerative disc disease: a finite element analysis. Comput Biol Med. 2021;128:104122.

16. Zou Y, Ji S, Yang HW, Ma T, Fang YK, Wang ZC, et al. Biomechanical evaluation of 2 endoscopic spine surgery methods for treating lumbar disc herniation: a finite element study. Neurospine. 2024;21(1):273–85.
17. Wu ZX, Sun HZ, Zhang Y, Xiao L, Zhao QL. Biomechanical Finite Element Analysis of Percutaneous Endoscopic Lumbar Discectomy via a Transforaminal Approach. World Neurosurg. 2024;185:e291–8.
18. Xue ST, Wu TL. Biomechanical performances of an oblique lateral Interbody Fusion Cage in models with different bone densities: a finite element analysis. Indian J Orthop. 2022;57(1):86–95.
19. Xiao ZT, Wang LY, Gong H, Zhu D. Biomechanical evaluation of three surgical scenarios of posterior lumbar interbody fusion by finite element analysis. Biomed Eng Online. 2012;11:31.
20. Lo CC, Tsai KJ, Zhong ZC, Chen SH, Hung CH. Biomechanical differences of Coflex-F and pedicle screw fixation combined with TLIF or ALIF–a finite element study. Comput Methods Biomech Biomed Engin. 2011;14(11):947–56.
21. Kang S, Park CH, Jung H, Lee S, Min YS, Kim CH, et al. Analysis of the physiological load on lumbar vertebrae in patients with osteoporosis: a finite-element study. Sci Rep. 2022;12(1):11001.
22. Yamamoto I, Panjabi MM, Crisco T, Oxland T. Three-dimensional movements of the whole lumbar spine and lumbosacral joint. Spine (Phila Pa 1976).
23. Choi G, Pophale CS, Patel B, Uniyal P. Endoscopic spine surgery. J Korean Neurosurg Soc. 2017;60(5):485–97.
24. Xu G, Zhang XX, Zhu MY, Yan Y, Zhang Y, Zhang JJ, et al. Clinical efficacy of transforaminal endoscopic discectomy in the treatment of recurrent lumbar disc herniation: a single-center retrospective analysis. BMC Musculoskelet Disord. 2023;24(1):24.
25. Benzakour T, Igoumenou V, Mavrogenis AF, Benzakour A. Current concepts for lumbar disc herniation. Int Orthop. 2019;43(4):841–51.
26. Li XH, Hu ZY, Cui J, Han YC, Pan J, Yang MJ, et al. Percutaneous endoscopic lumbar discectomy for recurrent lumbar disc herniation. Int J Surg. 2016;27:8–16.
27. Yao Y, Liu H, Zhang HY, Wang HG, Zhang C, Zhang ZF, et al. Risk factors for recurrent herniation after percutaneous endoscopic lumbar discectomy. World Neurosurg. 2017;100:1–6.
28. Bae JS, Lee SH. Transforaminal full-endoscopic lumbar discectomy in obese patients. Int J Spine Surg. 2016;10:18.
29. Ren GR, Liu L, Zhang P, Xie ZY, Wang PY, Zhang W, et al. Machine learning predicts recurrent lumbar disc herniation following percutaneous endoscopic lumbar discectomy. Global Spine J. 2024;14(1):146–52.
30. Dobran M, Nasi D, Paracino R, Gladi M, Costanza MD, Marini A, et al. Analysis of risk factors and postoperative predictors for recurrent lumbar disc herniation. Surg Neurol Int. 2019;10:36.
31. Mysliwiec LW, Cholewicki J, Winkelpleck MD, Eis GP. MSU classification for herniated lumbar discs on MRI: toward developing objective criteria for surgical selection. Eur Spine J. 2010;19(7):1087–93.
32. Li JC, Zhang XY, Xu WQ, Xi ZP, Xie L. Reducing the extent of facetectomy may decrease morbidity in failed back surgery syndrome. BMC Musculoskelet Disord. 2019;20(1):369.
33. Callaghan JP, McGill SM. Intervertebral disc herniation: studies on a porcine model exposed to highly repetitive flexion/extension motion with compressive force. Clin Biomech (Bristol). 2001;16(1):28–37.
34. Schmidt H, Kettler A, Heuer F, Simon U, Claes L, Wilke HJ. Intradiscal pressure, shear strain, and fiber strain in the intervertebral disc under combined loading. Spine (Phila Pa 1976). 2007;32(7):748–55.
35. Teichtahl AJ, Urquhart DM, Wang Y, Wluka AE, Wijethilake P, O'Sullivan R, et al. Fat infiltration of paraspinal muscles is associated with low back pain, disability, and structural abnormalities in community-based adults. Spine J. 2015;15(7):1593–601.
36. Yazici A, Yerlikaya T. The relationship between the degeneration and asymmetry of the lumbar multifidus and erector spinae muscles in patients with lumbar disc herniation with and without root compression. J Orthop Surg Res. 2022;17(1):541.

Publisher's note